
Since January 2020 Elsevier has created a COVID-19 resource centre with free information in English and Mandarin on the novel coronavirus COVID-19. The COVID-19 resource centre is hosted on Elsevier Connect, the company's public news and information website.

Bioelectrochemistry 143 (2022) 107982

Contents lists available at ScienceDirect

Bioelectrochemistry

journal homepage: www.elsevier.com/locate/bioelechem

# Carbon nanotube field-effect transistor (CNT-FET)-based biosensor for rapid detection of SARS-CoV-2 (COVID-19) surface spike protein S1

Mazin A. Zamzami [a,b,c,*], Gulam Rabbani [d], Abrar Ahmad [a], Ahmad A. Basalah [e], Wesam H. Al-Sabban [f], Saeyoung Nate Ahn [d,g,*], Hani Choudhry [a,b,c]

[a] Department of Biochemistry, Faculty of Science, King Abdulaziz University, Jeddah 21589, Saudi Arabia
[b] Cancer Metabolism and Epigenetic Unit, Faculty of Science, King Abdulaziz University, Jeddah 21589, Saudi Arabia
[c] Centre of Artificial Intelligence in Precision Medicines, King Abdulaziz University, Jeddah 21589, Saudi Arabia
[d] Nano Diagnostics & Devices (NDD), IT Medical Fusion Center, 350-27 Gumidae-ro, Gumi-si, Gyeongbuk 39253, Republic of Korea
[e] Department of Mechanical Engineering, College of Engineering & Islamic Architecture, Umm Al-Qura University, Makkah, Saudi Arabia
[f] Department of Information Systems, College of Computer and Information Systems, Umm Al-Qura University, Makkah, Saudi Arabia
[g] Fuzbien Technology Institute, 13 Taft Court, suite 222, Rockville, MD 20850, USA

ARTICLE INFO

*Article history:*
Received 23 June 2021
Received in revised form 10 October 2021
Accepted 12 October 2021
Available online 15 October 2021

*Keywords:*
Carbon nanotubes
Field-effect transistor
Biosensor
Electrical immunosensor
Severe acute respiratory syndrome coronavirus-2

ABSTRACT

The large-scale diagnosis of severe acute respiratory syndrome coronavirus 2 (SARS-CoV-2) is important for traceability and treatment during pandemic outbreaks. We developed a fast (2–3 min), easy-to-use, low-cost, and quantitative electrochemical biosensor based on carbon nanotube field-effect transistor (CNT-FET) that allows digital detection of the SARS-CoV-2 S1 in fortified saliva samples for quick and accurate detection of SARS-CoV-2 S1 antigens. The biosensor was developed on a $Si/SiO_2$ surface by CNT printing with the immobilization of a anti-SARS-CoV-2 S1. SARS-CoV-2 S1 antibody was immobilized on the CNT surface between the S-D channel area using a linker 1-pyrenebutanoic acid succinimidyl ester (PBASE) through non-covalent interaction. A commercial SARS-CoV-2 S1 antigen was used to characterize the electrical output of the CNT-FET biosensor. The SARS-CoV-2 S1 antigen in the 10 mM AA buffer pH 6.0 was effectively detected by the CNT-FET biosensor at concentrations from 0.1 fg/mL to 5.0 pg/mL. The limit of detection (LOD) of the developed CNT-FET biosensor was 4.12 fg/mL. The selectivity test was performed by using target SARS-CoV-2 S1 and non-target SARS-CoV-1 S1 and MERS-CoV S1 antigens in the 10 mM AA buffer pH 6.0. The biosensor showed high selectivity (no response to SARS-CoV-1 S1 or MERS-CoV S1 antigen) with SARS-CoV-2 S1 antigen detection in the 10 mM AA buffer pH 6.0. The biosensor is highly sensitive, saves time, and could be a helpful platform for rapid detection of SARS-CoV-2 S1 antigen from the patients saliva.


## 1. Introduction

The World Health Organization (WHO) announced on 11 March 2020 that the SARS-CoV-2 epidemic was a pandemic and a global health emergency [1]. It is well known that there have been three human pathogenic coronavirus outbreaks in the 21st century that triggered transmission and posed immense challenges to global public health and economic growth [2]. The three virus outbreaks were SARS-CoV in 2003 [3], MERS-CoV in 2012 [4], and the new SARS-CoV-2 in December 2019 [5]. Phylogenetic data analysis suggests that SARS-CoV-2 is further away from the SARS-CoV (79 %) and MERS-CoV (50 %) strains [6]. SARS-CoV-2 has a large positive-stranded RNA genome size of 29.8 kb that gives signals for encoding accessory and four structural proteins: spike glycoprotein (S), envelope (E), matrix (M), and nucleocapsid (NC) [7].

*Abbreviations:* AA, Ammonium acetate; ACE2, Angiotensin-converting enzyme 2; AuNPs, gold nanoparticles; BSA, Bovine serum albumin; CNT, Carbon nanotube; COVID-19, coronavirus disease 2019; EDC, 1-(3-dimethylaminopropyl)-3-ethylcar bodiimide hydrochloride; FET, field-effect transistor; $I_{DS}$, source-drain current; MERS-CoV, Middle East respiratory syndrome coronavirus; MES, 2-(*N*-morpholino) ethanesulfonic acid; NHS, *N*-hydroxysuccinimide; PBASE, 1-pyrenebutanoic acid succinimidyl ester; PBST, Phosphate-buffered saline containing 0.05% Tween-20; pI, Isoelectric point; SARS-CoV-1 and 2, severe acute respiratory syndrome coronavirus 1 and 2; S-D, source-drain; SEM, Scanning electron microscopy; Vds, source to drain voltage; Vg, gate voltage.

* Corresponding authors at: Department of Biochemistry, Faculty of Science, King Abdulaziz University, Jeddah 21589, Saudi Arabia (M.A. Zamzami) and Nano Diagnostics & Devices (NDD), IT Medical Fusion Center, 350-27 Gumidae-ro, Gumi-si, Gyeongbuk 39253, Republic of Korea (S.N. Ahn).

*E-mail addresses:* mzamzami@kau.edu.sa (M.A. Zamzami), nate.ahn@gmail.com (S. Nate Ahn).

https://doi.org/10.1016/j.bioelechem.2021.107982
1567-5394/

Among those, only spike (S) glycoprotein faces the outer structure on the virion body, which is highly immunogenic for the host and the best reliable biomarker for the diagnosis of SARS-CoV-2 infection [8–10]. S-protein monomer is folded and glycosylated by sialic acid at the distal end [11]. S-protein is cleaved by host proteases into two subunits, S1 and S2; the S1 subunit functions in host cell recognition, cell invasion, and antibody neutralization [12]. SARS-CoV-2 infection is mediated by the binding of the S1 subunit of spike (S) protein to the host cell receptor through the receptor-binding domain (RBD) present on the angiotensin-converting enzyme 2 (ACE2) [13,14]. SARS-CoV-2 inhaled through aerosol droplets binds to host cellular receptor ACE2 and targets activating proteases (for example, TMPRSS2, furin, and cathepsin L) for membrane fusion and reaches the host respiratory cells [15,16]. The virus easily spreads by touch, droplets, air contamination, the oral-fecal route, or blood, from mothers to newborns and animals to humans [17–19]. As a result the world increasingly needs diagnostic tools with the capability of identifying the infected individuals e.g. the source of infection.

Electrochemical biosensors are advantageous for sensing biomolecules because of their ability to detect biomarkers with accuracy, specificity and high sensitivity [20]. Previously electrochemical biosensors have been successfully used in medical diagnostics for the detection of viruses such as MERS-CoV [21], hepatitis C virus (HCV) [22], human influenza A virus H9N2 [23] and avian influenza virus (AIV) H5N1 [24]. Recently, Shao et al. developed a SARS-CoV-2 S antigen detection device based on a carbon nanotube field-effect transistor (CNT-FET) functionalized with anti-SARS-CoV-2 spike antibody with a detection range of 5.5 fg/mL to 5.5 pg/mL [25]. The real-time polymerase chain reaction (RT-PCR) is rigorously used for the diagnosis of SARS-CoV-2. RT-PCR is excellent in terms of sensitivity and selectivity, but can only be performed in well-equipped laboratory-based hospitals, requires costly chemicals, enzymes, spacious machinery, and requires up to 1–2 days. In order to detect SARS-CoV-2 quickly with high accuracy, a simple, sensitive, and low-cost biosensor is needed.

This research paper describes the development of a new CNT-FET-based biosensor for reliable, fast detection of SARS-CoV-2 S1 antigen with high selectivity and sensitivity. Here, we present a highly sensitive electrical immunosensor for the detection of SARS-CoV-2 S1 antigen using single wall carbon nanotubes (SWCNTs) deposited on the surface of $SiO_2$ between the S-D channel. The developed biosensor is based on the field-effect transistor (FET) technology, and its fabrication involves the immobilization of antibodies between the S-D sensing area. The newly developed CNT-FET immunosensor can detect SARS-CoV-2 S1 antigen, based on the change in source-drain current ($I_{DS}$), and the antigen-binding effect is characterized by a change in electrical signal (Scheme 1). The basic advantages of the FET-based biosensor are easy fabrication, fast sensing response, and ease of use because the dynamic real-time response can be acquired with low-cost digital readers that can be calibrated for different applications. Certainly, at central hospitals and testing centers, advanced and traditional equipment can analyze and diagnose SARS-CoV-2 infection with high accuracy and precision. In pandemic circumstances, CNT-FET-based biosensors could be helpful as potential detection devices for tracing SARS-CoV-2 infection at the mass level.

## 2. Materials and sample preparation

Single-wall CNTs with a length of 5 to 30 μm and diameter of 1 to 2 nm were purchased from NanoIntegris, Canada. SARS-CoV-2 spike/S1 subunit-His tag (Cat# 40591-V08H), SARS-CoV-1 spike/S1 subunit-His tag (Cat# 40150-V08B1) and MERS-CoV spike/S1 subunit His tag recombinant protein (Cat# 40069-V08H) were purchased from Sino Biological Inc., Beijing, China. Monoclonal rabbit anti-spike S1 antibody (40150-R007) was purchased from Sino Biological Inc, Beijing, China (antibody specificity was not validated with corresponding SARS-CoV-2 real positive virus saliva/serum sample). HRP-conjugated secondary antibody goat pAb to rabbit IgG was purchased from Abcam (ab6721). 1,2-dichlorobenzene (Cat# 240644), linker, 1-pyrenebutanoic acid succinimidyl ester (PBASE, Cat# 457078), bovine serum albumin (BSA, Cat# A7906), colloidal suspension of 20 nm diameter, thiolated PEG with terminal carboxylic acid functionalized gold nanoparticles (Cat#765511), coupling reagent 1-(3-dimethylaminopropyl)-3-ethylcarbodiimide hydrochloride (EDC, Cat#03450), and *N*-hydroxysuccinimide (NHS, Cat#130672) were purchased from Sigma Aldrich. The enhanced chemiluminescence (ECL, Pico System, Cat#ECL-PS250) solution was purchased from Dongin Biotech, Korea. The bare silicon wafer was purchased from Waferbiz, Korea. PVDF transfer membrane (Immobilon P) was purchased from Merck Millipore ltd., Korea. Deionized (DI) water 18.2 MΩ/cm, to make the buffer and washing solutions, was obtained with an MDM Wellix Plus water purifier system (MDM Corporation, South Korea). The other reagents procured in this study were of analytical purity standard and used without any further purification.

The buckypaper of carbon nanotubes (CNTs) 0.1 mg/mL was mixed into 1,2-dichlorobenzene and sonicated for 1 h at room temperature to achieve a black dark homogeneous suspension. The suspended CNTs solution was centrifuged for 30 min at 5000 rpm to remove large aggregates and bundles. The homogeneous CNTs suspension was loaded into an inkjet printer cartridge for printing on the $Si/SiO_2$ substrate. PBASE solution of 2 mM was prepared in methanol by vortex mixing for 1 h at room temperature to achieve complete mixing of PBASE crystal. Then 1 × phosphate-buffered saline (PBS) was prepared by mixing 10 mM $Na_2HPO_4$, 137 mM NaCl, 2.7 mM KCl, and 2.0 mM $KH_2PO_4$. The molarity of phosphate in 1 × PBS was 12 mM, because an important ingredient for the buffer is 10 mM $Na_2HPO_4$ and 2.0 mM $KH_2PO_4$. Fresh 5 % skim milk solution was prepared in 1 × PBST containing 0.05 % Tween-20. Fresh 1 % bovine serum albumin (BSA) blocking solution was prepared in 1 × PBS.

## 3. Experiment

### 3.1. CNT-FET device fabrication

Source and drain (S-D) electrodes of Ti 10 nm/Au 30 nm were patterned by a conventional photolithography method and lift-off technique. After leaving it for 1 h, the Si wafer was soaked in 1,2-dichlorobenzene, acetone, and methanol for 30 s for each co-solvent, and finally, DI water was used for rinsing and nitrogen ($N_2$) gas blowdown. A uniform CNT ink (separated semiconducting SWNTs at 0.1 mg/mL in 1,2-dichlorobenzene) was printed on $Si/SiO_2$ substrate by inkjet printer between the active areas of patterned electrodes. To fix the printed CNT pattern on the base material, it was hard baked on a hot plate at 120 °C in the vacuum oven for 10 min. To avoid direct contact with the S-D electrode metal surface and minimize the gate current leakage due to flowing antigen test solution an additional photolithography step was employed to make SU-8 passivation layer on the S-D electrode.

### 3.2. Electrical property measurements of CNT-FET device

In order to investigate the semiconductor electrical properties and sensing efficiency of the CNT-FET device, measurements were performed by a Keithley 3 probe station at room temperature. The semiconductor property of the CNT-FET biosensor was validated by

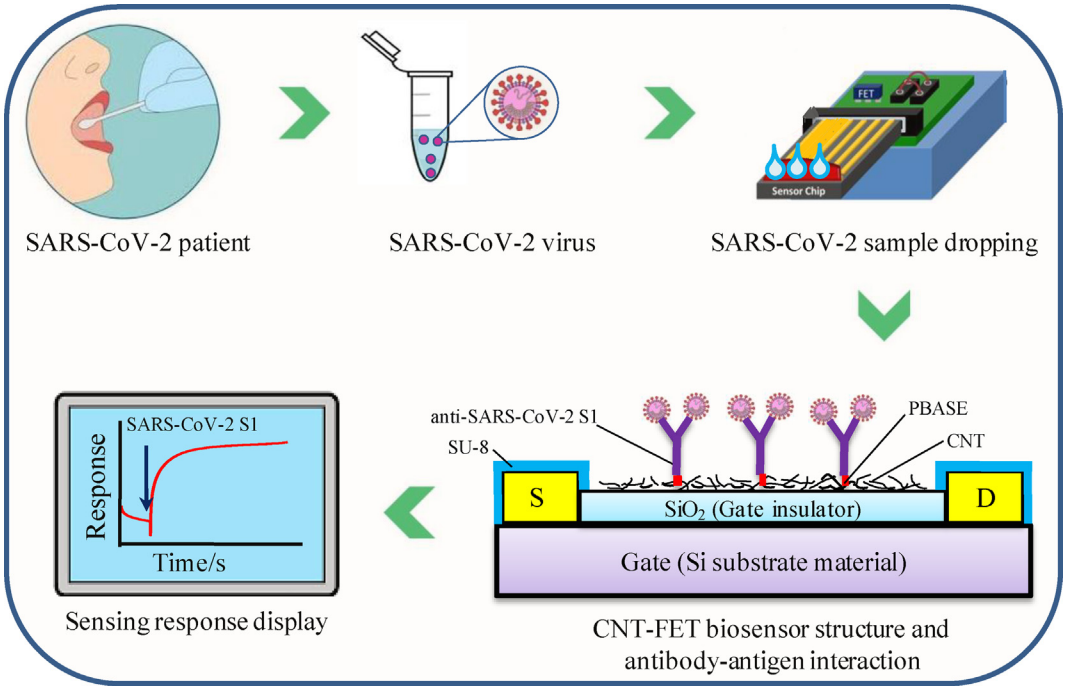


**Scheme 1.** Schematic diagram of CNT-FET biosensor and SARS-CoV-2 S1 testing steps. SWCNT as a sensing nanomaterial and anti-SARS-CoV-2 S1 immobilized on the CNT via PBASE (linker). The CNT-FET biosensor sense the SARS-CoV-2 spike protein based on the corresponding effects on the electrical signal properties.

acquiring the source-drain current ($I_{DS}$) versus gate voltage (Vg, −1.5 to 0.5 V) with a stable source-drain voltage (Vds = 0.5 V).

### 3.3. XPS measurement

X-ray photoelectron spectroscopy (XPS) spectra were acquired on a K-Alpha spectrometer (Thermo Fisher Scientific, USA). The machine is equipped with a micro-focused AlKα X-ray source (1486.6 eV) using a 10 mA emission current and an applied anode potential of 12 kV (120 W). The spectra were collected in constant analyzer energy mode with a pass energy of 200 eV for the survey. For reliable digital acquisition and data processing, Thermo Scientific Advantage software was used.

### 3.4. Surface modification and antibody immobilization on CNT-FET

Final CNT fabricated FET chips were soaked in 2 mM PBASE solution prepared in methanol for 1 h at room temperature. Subsequently, the sensing area of the CNT-FET chip was successively washed 3 times with pure methanol and DI water to remove the unbound excess PBASE (linkers) followed by $N_2$ gas blowdown. For functionalization, the monoclonal anti-SARS-CoV-2 S1 (1 μL of 100 μg/mL) in 0.01 × PBS solution was dropped on the channel area and left overnight at 4 °C in a humid chamber for binding with the PBASE-modified CNT surface. The unbound anti-SARS-CoV-2 S1 remains were removed by washing with 0.01 × PBST and DI water. The device was further exposed to 1 % bovine serum albumin (BSA) at room temperature in humid conditions for 20 min to block and inactivate nonspecific sites of the remaining nonfunctionalized CNTs and exposed $SiO_2$ substrate to ensure the binding of the specific target molecule. To eliminate excess BSA remaining after blocking, the device was thoroughly washed with 0.01 × PBST and DI water and dried by $N_2$ gas blowdown for 5 min. After complete drying, the CNT-FET device was connected to source, drain, and gate electrodes with a probe station for measurement of its post-treatment semiconductor behavior.

### 3.5. SARS-CoV-2 S1 protein conjugation with gold nanoparticles (AuNPs)

For this experiment, 500 μL of 20 nm (average size) thiolated PEG with terminal carboxylic acid (Thiol-PEG-COOH) functionalized colloidal gold nanoparticles (AuNPs) was taken from the stock vial and poured into a microcentrifuge tube. The AuNPs suspension stock vial carries an average of $6.54 \times 10^{11}$ particles/mL. The AuNPs suspension was mixed with 500 μL coupling buffer containing 20 mM EDC and 50 mM NHS dissolved in 0.1 M MES buffer pH 5.4. Then, the AuNP suspension containing the coupling mixture was incubated at room temperature for 24 h. The unreacted linker (EDC/NHS) was removed by centrifugation at 9660 × g for 30 min at 4 °C. After coupling of EDC/NHS linker with AuNPs, 100 μL of SARS-CoV-2 S1 antigen (50 μg/mL) was slowly added to the colloidal AuNPs suspension drop by drop with gentle stirring on a stir plate. Then, the AuNPs–SARS-CoV-2 S1 antigen mixture was allowed to react for 60 min at room temperature with gentle stirring. For blocking, 50 μL of freshly prepared 10 % BSA in DI water was added in colloidal AuNPs–SARS-CoV-2 S1 suspension and vortexed for 60 min at room temperature on a stir plate. After further incubation, the colloidal suspension was spun at 9660 × g for 30 min at 4 °C. The obtained supernatant was discarded and only the pelleted AuNPs–conjugated SARS-CoV-2 S1 antigen was resuspended and recovered by mixing with 2 mM borate buffer (pH 8.0, total volume was 100 μL). It was estimated that the final AuNPs–conjugated SARS-CoV-2 S1 antigen carried $6.37 \times 10^{11}$ particles/mL (supplementary information figure S1: by absorbance measurement at 520 nm). The AuNPs–conjugated SARS-CoV-2 S1 antigen was stored for further experimental use at 4 °C in an air-tight vial to prevent evaporation.

### 3.6. Sample preparation of SARS-CoV-2 S1 antigen conjugated AuNPs for scanning electron microscopy (SEM) imaging

CNT-FET chips with good S-D current versus gate voltage ($I_{DS}$-$V_{GS}$) signal properties were selected for SEM imaging

experiments. Step 1: The upper side of the CNT-FET chips (containing S-D and conducting CNT channel) was soaked in acetone solution for 10 min and air-dried at room temperature. For rigorous surface contamination removal, the acetone washing step was repeated 3 times. Step 2: Acetone-washed CNT-FET chips were soaked in 2 mM PBASE (linker) and left for 1 h at room temperature in air tight glass container. Step 3: After 1 h, CNT-FET chips were removed from the PBASE solution and washed 3 times with methanol and DI water followed by $N_2$ gas blowdown. Step 4: 1 μL of anti–SARS-CoV-2 S1 (100 μg/mL) in 0.01 × PBS solution was immobilized on the PBASE-modified CNT-FET biosensor and incubated for 4 h at room temperature in a humid chamber. Step 5: Washing with 0.01 × PBST was performed 5 times to remove unbound anti-SARS–CoV-2 S1 followed by air drying at room temperature. Step 6: To block and inactivate nonspecific sites, CNT-FET devices were further exposed to 1 % BSA and incubated at room temperature for 20 min in a humid chamber. Step 7: Washing with 0.01 × PBST was performed 5 times to remove unbound BSA traces, followed by air drying at room temperature. Step 8: 1 μL SARS-CoV-2 S1 antigen with conjugated AuNPs (diluted in 10 mM AA buffer, pH 6.0) was immobilized and incubated for 1 h at room temperature in a humid chamber. Step 9: Three times washing with 0.01 × PBST and DI water was performed to remove unbound AuNPs–conjugated SARS-CoV-2 S1 antigens, followed by a $N_2$ gas blow dry at room temperature. Step 10: The morphology and microstructure of CNT were characterized by field emission scanning electron microscope JEOL JSM-7610F (JEOL ltd, Akishima, Japan).

### 3.7. Western blot of SARS-CoV-2 surface spike glycoprotein S1

Western blot experiment was utilized to examine the specificity of anti-SARS-CoV-2 S1 and antigen binding. SARS-CoV-2 S1, SARS-CoV-1 S1, and MERS-CoV S1 with an antigen concentration of 1 μg/mL (lanes 1, 2, and 3) were separated under reducing conditions of 12 % polyacrylamide gel. After electrophoresis, protein bands were transferred from the SDS-PAGE gel to the PVDF membrane. The membrane was blocked in 1 × phosphate-buffered saline containing 0.05 % Tween-20 (PBST) and 5 % (w/v) skim milk and left overnight at 4 °C. After 3 washes with 1 × PBST, PVDF membrane was stained with SARS-CoV-2 (2019-nCoV) spike protein S1 primary antibodies at 1:5000 dilution (200 ng/mL) for 2 h in 5 % skim milk solution in 1 × PBST. After 3 washes with 1 × PBST, the membrane was further incubated in 5 % skim milk containing secondary antibody goat pAb to rabbit IgG conjugated to HRP (1:5000 dilution) for 60 min at room temperature on a rotating shaker plate. The membrane was washed 5 times with 1 × PBST to remove unbound remains. ECL solution was mixed in a 1:1 ratio following the proportions of solutions A and B provided by the manufacturer. ECL is a chemiluminescent substrate that detects horseradish peroxidase (HRP) conjugated secondary antibodies where light emission is proportional to the protein concentration. ECL consists of 2 reagents, reagent A (luminol) and reagent B (an enhancer). The PVDF membrane was placed on plastic film, freshly mixed ECL reagents A and B (1 mL each, total volume 2 mL) at a 1:1 ratio were added, and the membrane was incubated up to 3 min to complete the reaction. The PVDF membrane was lifted from the plastic film and transferred to the membrane cassette. The signal was exposed in the darkroom with an exposure time of 40 s, and the X-ray film was developed by immersing in the appropriate developing and fixing solutions for 5 min each.

### 3.8. Antigen sample preparation and antigen test

SARS-CoV-2 S1, SARS-CoV-1 S1 and MERS-CoV S1 antigen stocks were prepared in 10 mM ammonium acetate (AA) buffer at pH 6.0 and, to prevent denaturation, stored at 4 °C. The SARS-CoV-2 S1 antigen was diluted in 10 mM AA buffer at pH 6.0 with increasing concentrations (0.1, 1, 10, 100, and 5000 fg/mL). The CNT-FET device was connected to 3 probe station, and 0.8 μL of 10 mM AA buffer at pH 6.0 was dropped to equilibrate the $I_{DS}$ and achieve the stable baseline. After achieving a stable baseline of the biosensor, increasing concentrations of SARS-CoV-2 S1 antigen were sequentially dropped onto the S-D channel regions. The sample volume was 0.8 μL in each drop.

### 3.9. Selectivity measurements of the CNT-FET biosensor

A selectivity test experiment was performed to determine the biosensor's ability to select target molecules. Target SARS-CoV-2 S1 antigen and non-target SARS-CoV-1 S1 and MERS-CoV S1 antigens were tested using the anti-SARS-CoV-2 S1 immobilized on CNT-FET biosensor.

### 3.10. SARS-CoV-2 S1 fortified saliva preparation and electrical response measurement

For this experiment, 1 μL SARS-CoV-2 S1 antigen was added to 99 μL healthy human saliva sample to mimic a SARS-CoV-2-positive saliva sample and incubated for 30 min at 37 °C. In the fortified human saliva final concentration of SARS-CoV-2 S1 antigen was (0.1, 1, 10, 100, 1000, 2000, 3000, 4000 and 5000 fg/mL). These fortified saliva solution used as a test sample instead of a clinical SARS-CoV-2 positive sample. Then 1.0 μL SARS-CoV-2-positive simulated saliva sample was added to the anti-SARS-CoV-2 S1 functionalized CNT-FET biosensor and the electrical signal was read up to 60–120 s.

### 3.11. CNT-FET biosensor reproducibility and reusability test

Reproducibility tests of each biosensor were characterized by the various parameters for practical applications. For this, three batches (1, 2, and 3 batch) of fabricated CNT-FET biosensors were taken, each batch was replicated with saliva and fortified saliva and a total of 24 chips were selected and semiconductor property were validated by I-V measurements. The reproducibility was determined by the SARS-CoV-2 S1 fortified saliva and only saliva dropping experiment. The used concentration of SARS-CoV-2 S1 antigen was 100 fg/mL in 10 mM AA buffer of pH 6.0.

For the reusability experiment, different chips from the new batch were used after the antigen test was completed. The tested SARS-CoV-2 antigen and immobilized anti-SARS-CoV-2 S1 were removed from the biosensor sensing area by 5 times 0.01 × PBST washing. To fix the fabrication structure on the base material, it was hard baked on a hot plate at 120 °C in the vacuum oven for 10 min. After it was completely dry, S-D current versus gate voltage ($I_{DS}$-$V_{GS}$) measurement was again performed to see the semiconductor properties either retained or destroyed in the washing process. Further on the dried CNT-FET biosensor PBASE linker and anti-SARS-CoV-2 S1 were immobilized (the same steps are repeated as described in section 3.4). SARS-CoV-2 S1, SARS-CoV-1 S1 and MERS-CoV S1 antigen test measurements were again conducted S-D current versus time ($I_{DS}$-T) and acquired data of the CNT-FET biosensor was compared with the used and reused CNT-FET biosensor.

## 4. Results and discussion

### 4.1. Basic structure of the CNT-FET device and optical microscopy (OM)/SEM imaging

The basic structure of the field-effect transistor (FET) is shown in Fig. 1A. The complete fabricated CNT-FET device after a single

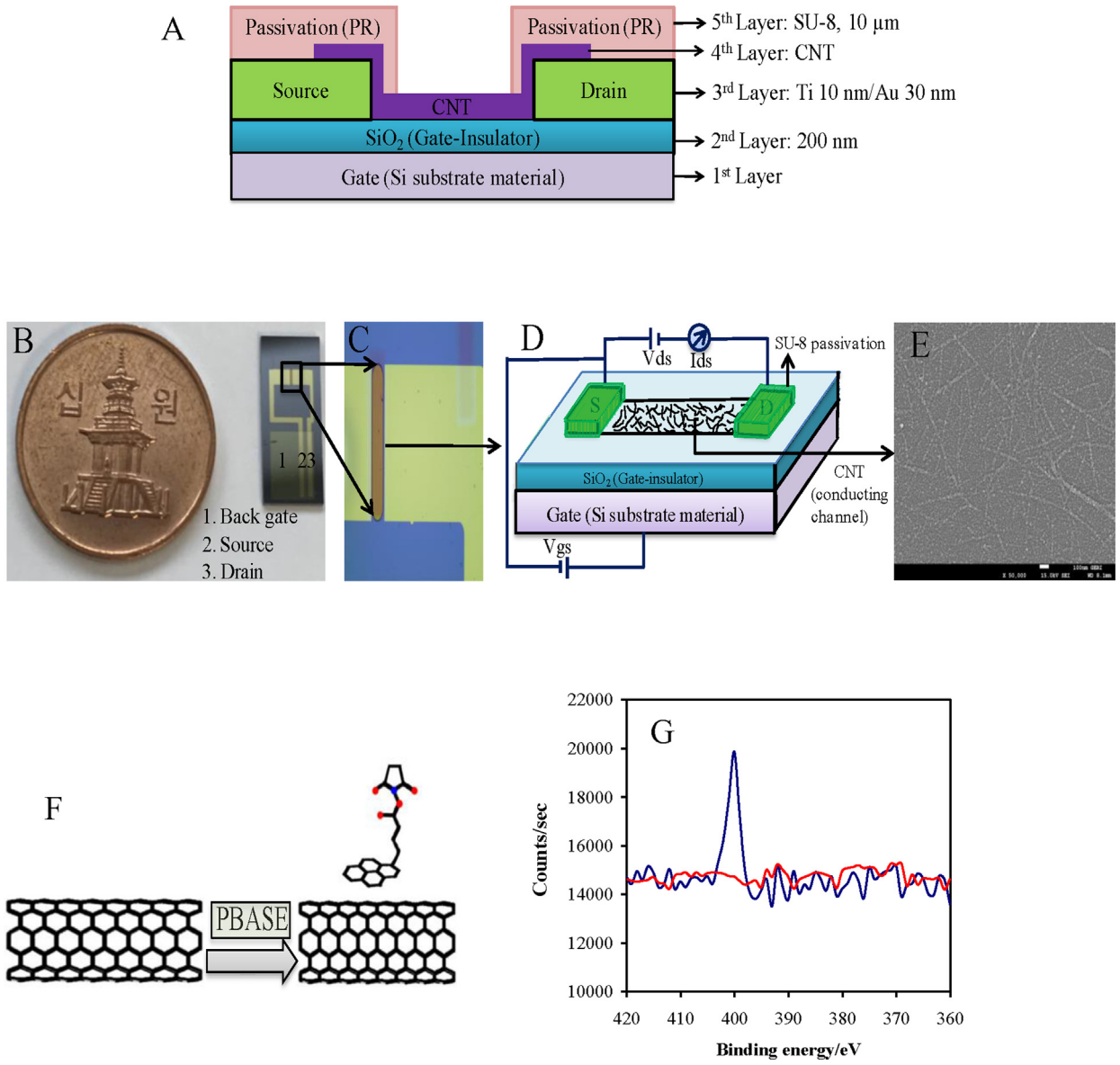


**Fig. 1.** **(A)** Schematic representation of CNT-FET device illustrating structural components and thickness of fabricated nanomaterial. The CNT network makes contact with metal electrodes (source-drain). A SU-8 photoresist on the source-drain electrodes is used to prevent leakage of gate current. **(B)** Optical image of single die CNT-FET device from wafer. **(C)** Optical microscope image of CNT-FET device showing source-drain electrodes. **(D)** Schematic structure of FET circuit diagram and CNT network situated between source-drain electrodes on conductive substrate. **(E)** SEM image of deposited CNT network on surface. **(F)** Surface functionalization of CNT-FET by 2 mM PBASE (linker). **(G)** XPS spectra of CNT-FET surface before (red line) and after PBASE treatment (blue line). Change in N1s peak at 400.2 eV assigned for PBASE was successfully modified the CNT surface.

die is shown in Fig. 1B. Optical microscopy (OM) was used to identify the locations of nanotubes bridging source-drain (S-D) electrode pairs in order to determine the fabrication process (Fig. 1C). Inkjet printing was used to deposite CNTs, random network on the $SiO_2$ surface between the S-D of the device. The schematic structure of the FET circuit diagram along with the CNT semiconductive network situated between S-D electrodes on the substrate is shown in Fig. 1D. The deposited CNT network characterized by SEM imaging is shown in Fig. 1E.

### 4.2. Characterization of CNT-FET surface

The basic mechanism of PBASE functionalization with CNT surface is shown in Fig. 1F. To confirm the CNT-FET biosensor surface modification and the presence of PBASE on the surface of the device, X-ray photoelectron spectroscopy (XPS) was employed. The peak height of XPS difference spectra can be used to confirm the absence or presence of functionalized PBASE on the CNT surface by analyzing the N1s peak at 400.2 eV. As seen in Fig. 1G, the bare surface did not show any peak increase at 400.2 eV, and after PBASE modification of the device, the N1s peak appeared at 400.2 eV. The binding energy values after N substitution were assigned in the range of 400.2 to 401.8 eV. These XPS results clearly suggest successful functionalization since the only source of nitrogen atoms in functionalized CNT is the PBASE molecule. The PBASE was immobilized on the surface of the carbon nanostructure by π-π non-covalent stacking between the six-membered ring of the CNT sidewall and the pyrene group of PBASE [26–28], while the succinimidyl ester group of the PBASE facing upward on the surface of CNT can react with an amine group of the target antibody and forms an amide bond [29].

### 4.3. SEM characterization of patterned CNT

The morphology of CNT from scanning electron microscopy (SEM) is shown in Fig. 2. Bare $SiO_2$ shows a clean surface (Fig. 2A). SEM images show the microstructure of the unaligned CNT needle like fine network (Fig. 2B). On a nanometer scale with open pores, the CNTs formed an interconnected and well-entangled porous network. Aligned CNT bundles with varying diameters are shown by scanning electron microscopy, averaging approximately 30 μm. To confirm the immobilization pattern of anti-SARS-CoV-2 S1 on the PBASE modified CNT-FET between the S-D channel area of the biosensor. On the dry surface of anti-SARS-CoV-2 S1 immobilized area, AuNPs–SARS-CoV-2 S1 conjugated antigen solution was applied, and AuNPs–conjugated SARS-CoV-2 S1 antigen was bound with the immobilized anti-SARS-CoV-2 S1 between the S-D channel area. Fig. 2C shows the sphere-like structure that proves the presence of AuNPs–conjugated SARS-CoV-2 S1 antigen. SEM images in Fig. 2D show the AuNP sizes in the range of 19.3 to 23 nm. The increased size of AuNPs was due to the binding of the highly glycosylated SARS-CoV-2 S1 antigen. These findings suggest that the SARS-CoV-2 S1 antibody was successfully immobilized on the biosensing area, and the formation of the antibody-antigen complex localized by AuNPs is illustrated in Fig. 2C.

### 4.4. Study of anti-SARS-CoV-2 S1 specificity by Western blot

To confirm the specificity of anti-SARS-CoV-2 S1 with target SARS-CoV-2 S1 antigen, a Western blotting experiment was performed. Western blot data of SARS-CoV-2 S1, SARS-CoV-1 S1 and MERS-CoV S1 antigens at a concentration of 1 μg/mL (lanes 1, 2, and 3) are shown in Fig. 3. A single distinct band recognizes the 77 kDa SARS-CoV-2 surface spike glycoprotein S1 antigen (lane 1). The increased molecular size was observed due to the high glycosylation of the S1 protein. The nonspecific SARS-CoV-1 S1 and MERS-CoV S1 antigens did not show binding with the anti-SARS-CoV-2 S1(lanes 2 and 3). These results indicate that the used anti-SARS-CoV-2 S1 was specific for the SARS-CoV-2 S1antigen.

### 4.5. Electrical characterization of the biosensor

Before any treatment, the transfer property of the CNT-FET device was characterized as the best fit for a p-type CNT-FET device, acting as a conductor with semiconductor properties (Supplementary figure S2). Oxygen and water molecules adsorbed on the CNT surface withdraw electrons from the CNT, which results in the p-type operation [30]. Due to variations in the amount of SWCNT deposition on the individual chips, small variations in $I_{DS}$ can be observed. The transistor output of the individual chips, however, is very similar because of the differences in SWCNT distribution density across the relatively small and reasonably comparable. The CNT-FET biosensor was electrically characterized after each functionalization step in dry conditions at room temperature. The semiconductor properties of the biosensor were characterized before the treatment (i.e., only CNT on the surface), after CNT surface modification by PBASE, and after antibody immobilization. No gate current leakage was observed, with almost zero $I_{DS}$, suggesting a superior p-type transistor compared to previous reports [31].

The graph in Fig. 4A (black line) shows the source-drain current ($I_{DS}$) versus source gate voltage ($V_{GS}$) of the bare CNT-FET surface at a constant voltage of −1.5 V. As data shown in Fig. 4A, the electrical graph of bare CNT shows that as the gate voltage moved from positive to negative, there was a sharp increase in $I_{DS}$ (black line). The continuous increase in $I_{DS}$ as a change in $V_{GS}$ (positive to negative) indicates that the fabricated device exhibits a typical feature of the

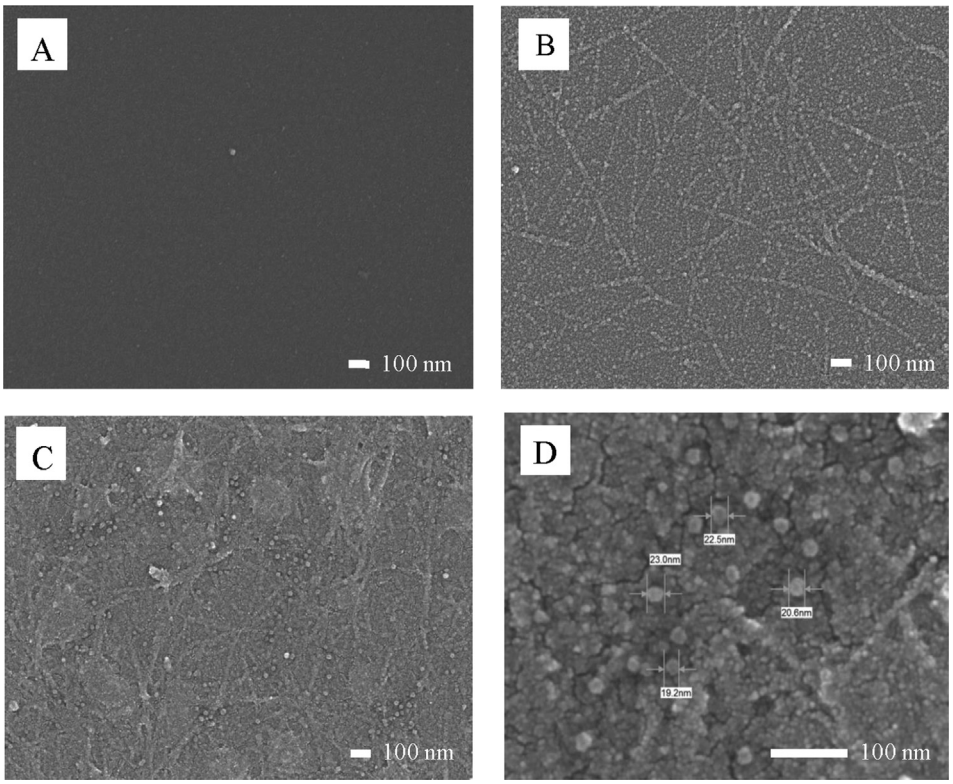


**Fig. 2.** Scanning electron photographs of channel area: **(A)** bare $SiO_2$ surface, **(B)** Bare surface after CNT printing, and **(C)** PBASE modification, anti-SARS-CoV-2 S1 immobilization, and binding of AuNPs–conjugated SARS-CoV-2 S1 antigen. **(D)** Enlarged image at 200,000 × magnification to measure gold nanoparticle size in the nm range.

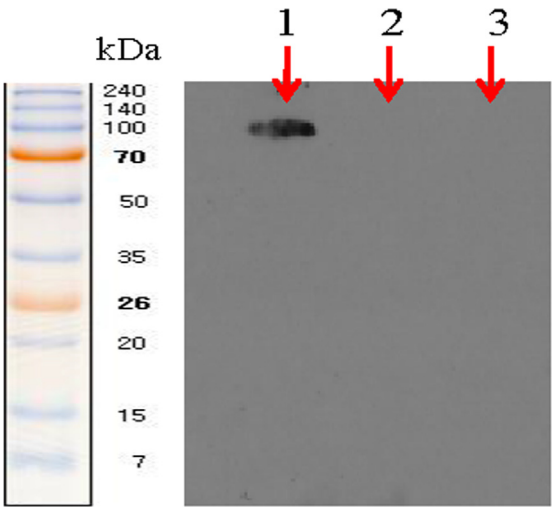


**Fig. 3.** Western blot images showing the detection of SARS-CoV-2 S1 by anti-SARS-CoV-2 S1-mAb antibodies. Lanes 1, 2, 3 represent loaded recombinant SARS-CoV-2 S1, SARS-CoV-1 S1, and MERS-CoV S1 antigens. For each antigen concentration, 1 μg/mL sample was loaded in SDS-PAGE.

p-type FET. The CNT-FET biosensor requires a linker molecule (PBASE) between the antibody and the CNT surface. After 2 mM PBASE treatment, the electrical behavior of the PBASE-functionalized CNT-FET biosensor was changed, that confirming the chosen linker molecule successfully modified the CNT surface (Fig. 4A red line).

SARS-CoV-2 S1 (1 μL of 100 μg/mL) antibody diluted in 0.01 × PBS was then exposed to the PBASE-modified CNT surface. After anti-SARS-CoV-2 S1 immobilization, surface was washed and dried in $N_2$ gas blow and the $I_{DS}$ of the CNT-FET biosensor was measured, and depleted drain current indicated that the antibody was successfully immobilized on the biosensor surface (Fig. 4A light blue line). Antibody immobilization leads to a 10–50 % decrease in ON-state current because of enhanced electron dispersion from crowded and more complex chemical environments along the CNT-FET source-drain channel area [32]. In each of these steps, the mobility of the CNT-FET device generally decreases by a small amount, as there are additional sources of dispersion of the charge carrier [33]. Garcia-Aljaro et al. reported that the decrease in $I_{DS}$ of the biosensor, that is, the increase in resistance, is due to the accumulation of negative charge from the immobilized antibodies on the biosensor [34]. Based on the same modification and attachment chemistry, changes in $I_{DS}$ versus $V_{GS}$ induced by the functionalization process were consistent with previously reported findings [35]. The mechanism of source-drain current ($I_{DS}$) decrease in carbon nanotube transistors may arise from the electrostatic gating effect and the Schottky barrier effect [36]. On the dry surface of the CNT-FET biosensor 1 μL of SARS CoV-2 S1 antigen was droped on the immobilized anti-SARS CoV-2 S1 and $I_{DS}$ of the CNT-FET biosensor was measured. As shown in Fig. 4A (green line), depleted drain current indicated that the SARS CoV-2 S1 antigen solution was strongly binds with immobilized anti-SARS CoV-2 S1 on the biosensor surface.

### *4.6. Determination of response time, detection limit, and detection range of CNT-FET biosensor*

The CNT-FET biosensor response time, limit of detection, and detection range were characterized by loading of target antigen (SARS-CoV-2 S1) at serially increased concentrations. The anti-SARS-CoV-2 S1 immobilized CNT-FET biosensor was used in systematic electrical signal measurements. First, at 10 *sec*, 0.8 μL of 10 mM (AA) buffer solution at pH 6.0 was dropped on the sensor to equilibrate the source-drain current ($I_{DS}$). After achieving a stabile $I_{DS}$ signal, continuously increasing SARS-CoV-2 S1 antigen concentrations (0.8 μL each drop) were loaded. The real-time response with increasing concentration of SARS-CoV-2 S1 antigen added every 50 s was recorded after achieving saturation of the observed $I_{DS}$. Each concentration of SARS-CoV-2 S1 antigen generated a characteristic spike and saturation, seen in all tested antigen concentrations (Fig. 4B).

A calibration curve was plotted as a function of SARS-CoV-2 S1 antigen concentration against normalized sensor response ($\Delta I/I_o$), shown in Fig. 4C. These results indicate that the CNT-FET biosensor detection lies in the range of 0.1 to 5000 fg/mL. The calibration curve indicates that the sensing response starts becoming saturated from 100 fg/mL of SARS-CoV-2 S1 antigen concentration; however, little increase in $I_{DS}$ was observed above a 100 fg/mL concentration. The limit of detection (LOD) was determined in the only linear portion of the curve based on the dose-dependent sensor response (Supplementary information). The LOD of the biosensor was 4.12 fg/mL in 10 mM (AA) buffer solution of pH 6.0. The sensitivity of the CNT-FET biosensor (immunochemical method) is non-linear at increasing SARS-CoV-2 S1 antigen concentration, probably the immobilized antibody number on the CNT surface is limited.

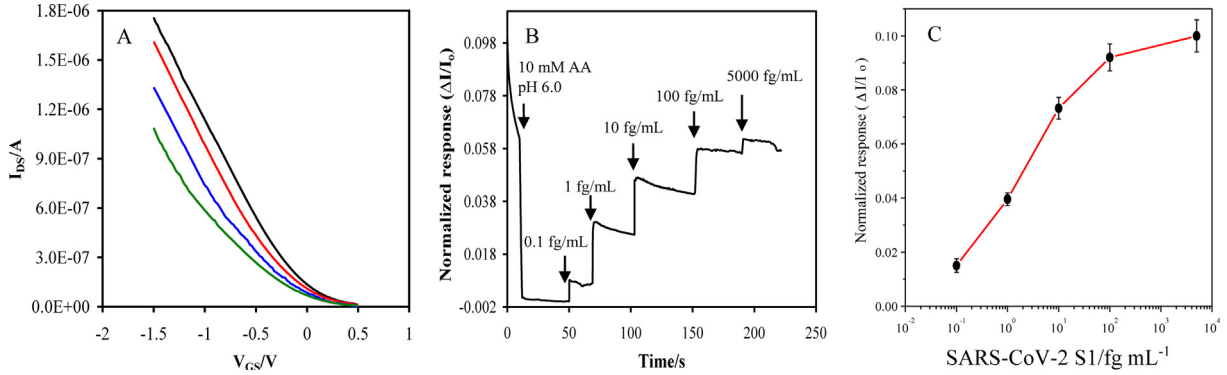


**Fig. 4. (A)** I-V characteristics of CNT-FET device at each biochemical treatment steps. Source-drain current ($I_{DS}$) versus gate voltage (Vg) characteristics of bare CNT-FET (black line). After 2 mM PBASE modification and I-V characterstics of the CNT-FET (red line). SARS-CoV-2 S1 antibody immobilized CNT-FET surface (light blue) and SARS-CoV-2 S1 antigen drop (green line). The 100 fg/mL SARS-CoV-2 S1 was prepared in10 mM AA buffer of pH 6.0. All the transfer characteristics are measured under ambient conditions. **(B)** Real time senror response characteristics after dropping increasing concentration (0.1, 1, 10, 100, and 5000 fg/mL) of SARS-CoV-2 S1 antigen. **(C)** Calibration curve after normalizing biosensor response versus applied concentration of target SARS-CoV-2 S1 antigen. Fixed drain-source voltage (Vds = 0.5 V) and Vg = -1.5 V. Error bars represent the standard deviation of three biosensor replicates. Each experiment was repeated a minimum of three times and typical results are shown.

Recently, Seo et al. fabricated a graphene-based FET biosensor for instant detection of SARS-CoV-2 spike S1 protein using monoclonal antibody immobilized, which had a LOD of 1 fg/mL [37]. The variation in LOD values of graphene and CNT-FET was due to the varying amount of semiconducting graphene and CNT in the device fabrication. Table 1 presents the data on SARS-CoV-2 detection by various biosensors reported in recent years. The summarized parameters collected from the relevant publications as shown in Table 1 include the analyzed biomarker target, LOD, measurement range, time required for final result generation, and compared with the results of this study on detection of SARS-CoV-2 S1. Our biosensor is highly sensitive comparing with the other reported biosensors. The sensitivity and time response of the biosensor varies with the number of immobilized detecting antibodies on the semiconducting CNT layer [38]. The dimension and width of the S-D may be other parameters that are responsible for the sensitivity of the biosensor [39].

### 4.7. Physiochemical properties of the SARS-CoV-2, SARS-CoV-1, and MERS-CoV spike proteins

The SARS-CoV-2 S1 antigen is positively charged (pI = 8.27) [40], and the SARS-CoV-2 S antigen is negatively charged (pI = 6.24) at neutral pH [25]. Table 2 summarizes the physicochemical properties of the SARS-CoV-2, SARS-CoV-1, and MERS-CoV spike proteins. The SARS-CoV-2 S1, SARS-CoV-1 S1, and MERS-CoV S1 antigens carry a net charge of + 5, −8, and −7, respectively, at pH 7.0 (Table 2). Based on these data, it was concluded that the SARS-CoV-2 S1 antigen carries more positive charge than the other two antigens at neutral pH. The SARS-CoV-2 S1 antigen was prepared in 10 mM AA buffer at pH 6.0. At this acidic pH, the antigen was more protonated and carried a net charge of + 13. This increased positive charge (+13) on the antigen strongly binds with the SARS-CoV-2 S1 antibody and generates a strong $I_{DS}$ response.

### 4.8. Selectivity study of the CNT-FET biosensor

Practically, a biosensor should be not only sensitive but also selective to a specific antigen. Selectivity is an important parameter in immunosensor applications because of the complex composition of biomolecules. Therefore, to confirm the selectivity of the CNT-FET biosensor, a control set of specific (SARS-CoV-2 S1) and non-specific (SARS-CoV-1 S1 and MERS-CoV S1) antigens were tested under identical experimental conditions. Fig. 5A shows the normalized biosensor response of the tested antigens prepared in 10 mM AA buffer at pH 6.0. First, after running the test, at time 10 s, the 10 mM AA buffer was dropped to stabilize the $I_{DS}$ of the CNT-FET biosensor. After $I_{DS}$ stabilization up to 50 s, the MERS-CoV S1 antigen was loaded on the biosensor. After saturation of the $I_{DS}$ signal, the SARS-CoV-1 S1 antigen was again dropped (Fig. 5A). These negative control experiments provide strong evidence that the no signal response of the CNT-FET biosensor reflects a highly selective response against non-specific antigens that reavels a non-specific binding. Immobilized anti-SARS-CoV-2 S1 recognized the target antigen, not the two tested non-specific antigens (Fig. 5B). SARS-CoV-2 S1 antibodies binding with specific antigens produced far greater changes in the $I_{DS}$ signal than the non-specific antigens. For particular antigen–antibody pairs, the CNT surface showed high electron transport properties compared to the non-specific pairs. These findings show a reduced normalized biosensor response by 8 to 9.5 % compared with specific antigen–antibody pairs.

Saliva samples with and without SARS-CoV-2 S1 antigen were tested. There was no significant change in $I_{DS}$ after dropping of non-fortified saliva on the biosensor (Fig. 5C). Saliva without SARS-CoV-2 S1 antigen showed a negligible response and did not show binding with immobilized anti-SARS-CoV-2 S1. However, saliva with SARS-CoV-2 S1 antigen showed a strong binding response with immobilized anti-SARS-CoV-2 S1. The concentration-dependent SARS-CoV-2 S1 fortified saliva was tested to see the biosensor response. As shown in Fig. 5D the sensor response was dependent on the SARS-CoV-2 S1 concentration present in the fortified saliva. The sensor response was almost saturated at 4000–5000 fg/mL SARS-CoV-2 S1 fortified saliva. These results indicate that the sensor response data is very similar as discussed in section 4.6.

### 4.9. Reproducibility and reusability study of the CNT-FET biosensor

Furthermore, the reproducibility tests of each biosensor are needed to characterize the parameters for practical applications.

**Table 2**
Molecular weight (Mw), net charge, isoelectric point (pI), and comparative physiochemical properties of spike protein of SARS-CoV-2, SARS-CoV-1, and MERS-CoV. Summarized values are predicted by online ProtParam tool (https://web.expasy.org/protparam/) [45].

| Properties | SARS-CoV-2 | SARS-CoV-1 | MERS-CoV |
|---|---|---|---|
| Spike (S) protein, UniProt ID | P0DTC2 | P59594 | A0A140AYZ5 |
| Spike protein sequence length | 1273 | 1255 | 1353 |
| Molecular weight (kDa) | 141.1 | 139.1 | 149.4 |
| Spike (S1/S2) protein cleavage site | R685/S686 | R667/S668 | R751/S752 |
| Spike protein net charge | −7 | −16 | −17 |
| S1 subunit net charge | +5 | 8 | −7 |
| S2 subunit net charge | −12 | −8 | −10 |
| S protein isoelectric point (pI) | 6.24 | 5.56 | 5.73 |
| S1 subunit isoelectric point (pI) | 8.27 | 5.67 | 5.98 |
| S2 subunit isoelectric point (pI) | 5.25 | 5.45 | 5.46 |
| RBD sequence length | sequence 333–526 | sequence 306–527 | sequence 367–606 |
| RBD net charge | +2 | +4 | −3 |

**Note:** ProtParam tool does not consider post-translational modification in the physiochemical parameter calculations. These estimated values should be followed with caution.

**Table 1**
Performance comparison of previously developed biosensor for SARS-CoV-2 target biomarker, detection method, LOD, detection range, and time required to generate final test result.

| Biomarker | Detection method | LOD | Detection range | Detection time | Ref. |
|---|---|---|---|---|---|
| SARS-CoV-2 spike protein (S) | CNT-FET | 5.5 fg/mL | 5.5 fg/mL to 5.5 pg/mL | 2 min | [25] |
| SARS-CoV-2 spike protein (S1) | Graphene-FET | 1 fg/mL | 1 fg/mL to 10 pg/mL | 5–8 min | [39] |
| SARS-CoV-2 nucleic acid/SARS-CoV-2 thiol-cDNA | Optical LSPR | 0.22 pM | 0.10 pm to 1.0 μM | 15–20 min | [41] |
| SARS-CoV-2 spike RBD | SWCNT intrinsically near-infrared (nIR) fluorescence | 12.6 nM | Not determined | 5 *sec* | [42] |
| SARS-CoV-2 spike protein (S) | Graphite electrode functionalized with AuNPs-cys | 229 fg/mL | 1 pg/mL to 1 ng/mL | 6.5 min | [43] |
| SARS-CoV-2 spike protein (S) | Tungsten diselenide ($WSe_2$) based-FET | 25 fg/μL | 25 fg/μL to 10 ng/μL | 2 min | [44] |
| SARS-CoV-2 spike protein (S1) | CNT-FET | 4.12 fg/mL | 0.1 fg/mL to 5.0 pg/mL | 2–3 min | This work |

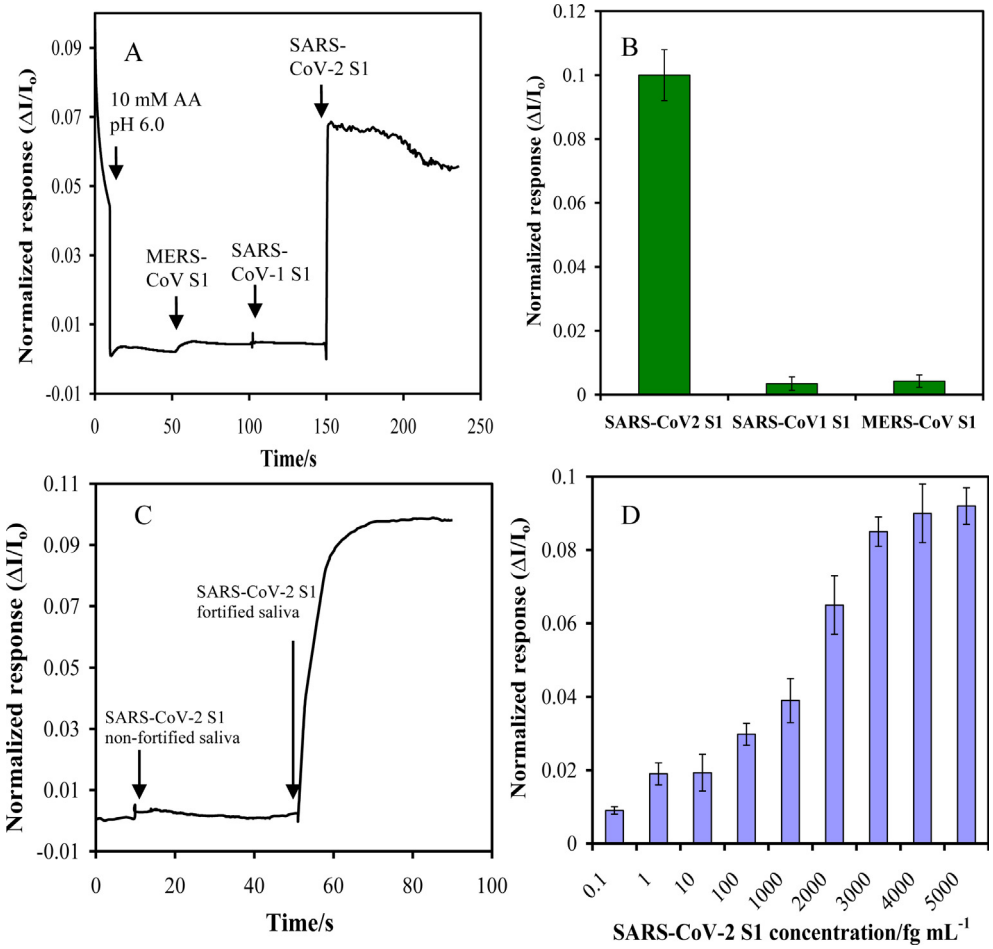


**Fig. 5.** **(A)** Real-time biosensor response for selectivity test of target SARS-CoV-2 S1 and non-target SARS-CoV-1 S1 and MERS-CoV S1 antigens. Antigen concentration was 100 fg/mL, prepared in 10 mM AA buffer at pH 6.0. **(B)** Normalized response ($\Delta I/I_o$) of target SARS-CoV-2 S1 and non-target SARS-CoV-2 S1 and MERS-CoV S1 antigens. Error bars represent the standard deviation of three biosensor replicates. Each experiment was repeated a minimum of three times and typical results are shown. **(C)** Normalized real-time biosensor response ($\Delta I/I_o$) versus time characteristics after SARS-CoV-2 S1 non-fortified and fortified saliva dropping. The used antigen concentration in fortified saliva was 100 fg/mL **(D)** Normalized real-time biosensor response ($\Delta I/I_o$) versus SARS-CoV-2 S1 antigen (0.1, 1, 10, 100, 1000, 2000, 3000, 4000 and 5000 fg/mL) fortified saliva. Error bars represent the standard deviation of three biosensor replicates. Each experiment was repeated a minimum of three times and typical results are shown.

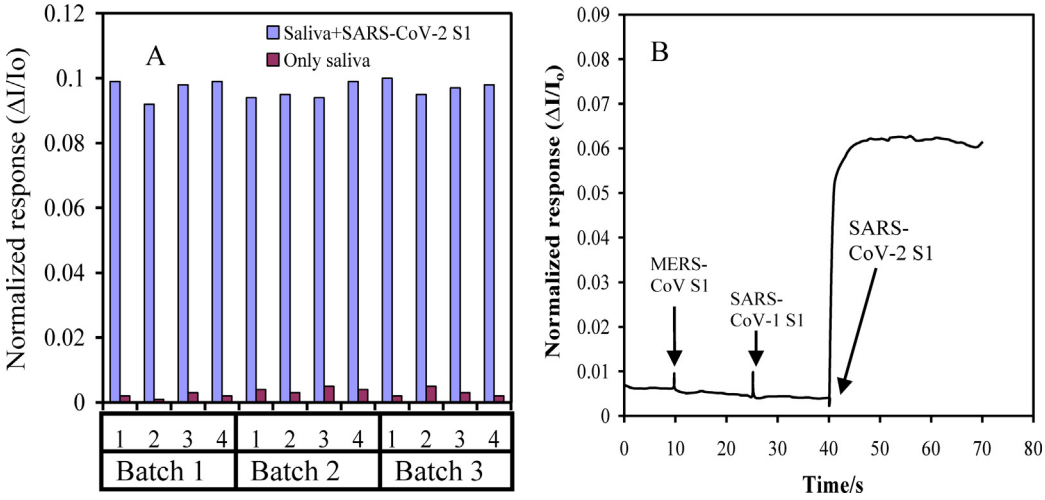


**Fig. 6.** **(A)** CNT-FET reproducibility test of 24 CNT-FET biosensors from 3 batches. 12 CNT-FET used for SARS-CoV-2 S1 fortified saliva and 12 CNT-FET used for only saliva test. Fixed drain-source voltage (Vds = 0.5 V) and Vg = -1.5 V were applied in the electrical signal measurements. **(B)** Normalized real-time biosensor response ($\Delta I/I_o$) versus time characteristics after 0.01 × PBST washing and drying (reused CNT-FET biosensor). Target SARS-CoV-2 S1 and non-target SARS-CoV-1 S1 and MERS-CoV S1 antigens were tested. Each antigens 100 fg/mL were prepared in10 mM AA buffer of pH 6.0.

Because reproducibility is one of the key factors that affecting the practical application of electrochemical immunosensors. Therefore, the reproducibility of fabricated CNT-FET biosensors from three batches (1, 2, and 3) was tested under the identical experimental condition by the SARS-CoV-2 S1 antigen dropping experiment (Fig. 6A). The obtained results demonstrate that all tested CNT-FET biosensors fabricated in all three batches exhibited very similar SARS-CoV-2 S1 antigen responses. The relative standard deviation (RSD) was estimated to be 2.65 % based on the generated electrical signal of the twelve replicates of SARS-CoV-2 S1 fortified saliva (Fig. 6A). Thus, these results indicate that fabricated CNT-FET biosensors have stable and good reproducibility for antigen recognition.

For the reusability experiment of CNT-FET-biosensor, SARS-CoV-2 S1 antigen tested biosensor was washed 5 times with 0.01 × PBST to clean the bound SARS-CoV-2 S1 antigen with anti-SARS-CoV-2 S1 and dried with $N_2$ gas blow. The MERS-CoV S1, SARS-CoV-1 S1 and SARS-CoV-2 S1 antigens were tested and the observed sensor response showing that after one use still fabricated material was stable and not damaged in the washing process. The normalized sensor response drop of SARS-CoV-2 S1 was 0.068, however in the reused biosensor the normalized sensor response was 0.062 (Fig. 5A and 6B). Based on the comparison of normalized sensor response (Fig. 5A and 6B), it was concluded that the sensitivity of the biosensor was decreased by 8.82 % (Fig. 6B). With less than 10 % of sensor response decrease, the regeneration step was working quite well for the developed system. The biosensor reusability response depends on the retained CNT-FET fabricated materials and the biosensor offers 91.18 % retained or higher sensing response.

## 5. Conclusion

We designed and successfully developed a very sensitive, selective, and quantifiable CNT-FET based antibody functionalized biosensor for SARS-CoV-2 S1 antigen detection in buffer solution and not in real samples. The biosensor was fabricated and operated under the p-type channel depletion principle. The source-drain metal electrodes were passivated by SU-8 photoresist to diminish direct contact with applied antigen samples and prevent a short circuit of the electrical components. The device showed excellent semiconductor properties. The quick response of the antigen drop confirms that source-drain semiconducting channels were quite sensitive to the transfer of electrons during antigen–antibody interaction. The CNT surface of the biosensor was modified by PBASE linker molecules, and anti-SARS-CoV-2 S1 were immobilized on the PBASE layer. The biosensing responses were rapid (minutes) and produced reliable, reproducible results. Antigen-specific concentration-dependent sensing response over a broad range of concentrations (0.1 to 5000 fg/mL) was shown in the calibration experiments. The CNT-FET biosensor is highly sensitive and able to discriminate SARS-CoV-2 S1, SARS-CoV-1 S1, and MERS-CoV S1 antigens, indicating good selectivity to SARS-CoV-2 S1. The experimental data indicate that the biosensor can be a good, low-cost biosensor for rapidly testing people for SARS-CoV-2 infection that is easy to handle. Thus the developed biosensor is inexpensive, simple, versatile, and easy to use, can be a prototype for SARS-CoV-2 S1 antigen detection and diagnosis of SARS-CoV-2 infection.

## Declaration of Competing Interest

The authors declare that they have no known competing financial interests or personal relationships that could have appeared to influence the work reported in this paper.

## Acknowledgments

The authors would like to acknowledge King Abdulaziz City for Science and Technology (General Directorate for Research and Innovation Support (GDRIS)) at King Abdulaziz University, Jeddah, Saudi Arabia, for financial support. The grant for this work was allocated through a fast-track program for COVID-19 research, project no. 5-20-01-009-0074.

## Appendix A. Supplementary material

Supplementary data to this article can be found online at https://doi.org/10.1016/j.bioelechem.2021.107982.

## References

[1] WHO Director-General's opening remarks at the media briefing on COVID-19 - 11 March 2020, (2020).
[2] J. Cui, F. Li, Z.-L. Shi, Origin and evolution of pathogenic coronaviruses, Nat Rev Microbiol 17 (3) (2019) 181–192.
[3] K. Stadler, V. Masignani, M. Eickmann, S. Becker, S. Abrignani, H.-D. Klenk, R. Rappuoli, SARS-beginning to understand a new virus, Nat Rev Microbiol 1 (3) (2003) 209–218.
[4] Z.A. Memish, S. Perlman, M.D. Van Kerkhove, A. Zumla, Middle East respiratory syndrome, Lancet 395 (10229) (2020) 1063–1077.
[5] N.a. Zhu, D. Zhang, W. Wang, X. Li, B.o. Yang, J. Song, X. Zhao, B. Huang, W. Shi, R. Lu, P. Niu, F. Zhan, X. Ma, D. Wang, W. Xu, G. Wu, G.F. Gao, W. Tan, A novel coronavirus from patients with Pneumonia in China, 2019, N Engl J Med 382 (8) (2020) 727–733.
[6] K.B. Anand, S. Karade, S. Sen, R.M. Gupta, SARS-CoV-2: Camazotz's Curse, Med J Armed Forces India 76 (2) (2020) 136–141.
[7] H. Wang, X. Li, T. Li, S. Zhang, L. Wang, X. Wu, J. Liu, The genetic sequence, origin, and diagnosis of SARS-CoV-2, Eur J Clin Microbiol Infect Dis 39 (9) (2020) 1629–1635.
[8] H. Yao, Y. Song, Y. Chen, N. Wu, J. Xu, C. Sun, J. Zhang, T. Weng, Z. Zhang, Z. Wu, L. Cheng, D. Shi, X. Lu, J. Lei, M. Crispin, Y. Shi, L. Li, S. Li, Molecular architecture of the SARS-CoV-2 virus, Cell 183 (3) (2020) 730–738.e13.
[9] P. Zhao, J.L. Praissman, O.C. Grant, Y. Cai, T. Xiao, K.E. Rosenbalm, K. Aoki, B.P. Kellman, R. Bridger, D.H. Barouch, M.A. Brindley, N.E. Lewis, M. Tiemeyer, B. Chen, R.J. Woods, L. Wells, Virus-receptor interactions of glycosylated SARS-CoV-2 spike and human ACE2 Receptor, Cell Host Microbe 28 (4) (2020) 586–601.e6.
[10] X. Ou, Y. Liu, X. Lei, P. Li, D. Mi, L. Ren, L. Guo, R. Guo, T. Chen, J. Hu, Z. Xiang, Z. Mu, X. Chen, J. Chen, K. Hu, Q. Jin, J. Wang, Z. Qian, Characterization of spike glycoprotein of SARS-CoV-2 on virus entry and its immune cross-reactivity with SARS-CoV, Nat Commun 11 (1) (2020) 1620.
[11] L. Wang, Y.e. Xiang, Spike glycoprotein-mediated entry of SARS coronaviruses, Viruses 12 (11) (2020) 1289, https://doi.org/10.3390/v12111289.
[12] S. Xiaojie, L. Yu, Y. Lei, Y. Guang, Q. Min, Neutralizing antibodies targeting SARS-CoV-2 spike protein, Stem Cell Res 50 (2020) 102125.
[13] Y. Huang, C. Yang, X.F. Xu, W. Xu, S.W. Liu, Structural and functional properties of SARS-CoV-2 spike protein: potential antivirus drug development for COVID-19, Acta Pharmacol Sin 41 (9) (2020) 1141–1149.
[14] A.C. Walls, Y.-J. Park, M.A. Tortorici, A. Wall, A.T. McGuire, D. Veesler, Structure, function, and antigenicity of the SARS-CoV-2 spike glycoprotein, Cell 181 (2) (2020) 281–292.e6.
[15] H.F. Florindo, R. Kleiner, D. Vaskovich-Koubi, R.C. Acúrcio, B. Carreira, E. Yeini, G. Tiram, Y. Liubomirski, R. Satchi-Fainaro, Immune-mediated approaches against COVID-19, Nat Nanotechnol 15 (8) (2020) 630–645.
[16] M.D. Johansen, A. Irving, X. Montagutelli, M.D. Tate, I. Rudloff, M.F. Nold, N.G. Hansbro, R.Y. Kim, C. Donovan, G. Liu, A. Faiz, K.R. Short, J.G. Lyons, G.W. McCaughan, M.D. Gorrell, A. Cole, C. Moreno, D. Couteur, D. Hesselson, J. Triccas, G.G. Neely, J.R. Gamble, S.J. Simpson, B.M. Saunders, B.G. Oliver, W.J. Britton, P.A. Wark, C.A. Nold-Petry, P.M. Hansbro, Animal and translational models of SARS-CoV-2 infection and COVID-19, Mucosal Immunol 13 (6) (2020) 877–891.
[17] G. Kutti-Sridharan, R. Vegunta, B.P. Mohan, V.R.P. Rokkam, SARS-CoV2 in different body fluids, risks of transmission, and preventing COVID-19: A comprehensive evidence-based review, Int J Prev Med 11 (2020) 97.
[18] E.A. Meyerowitz, A. Richterman, R.T. Gandhi, P.E. Sax, Transmission of SARS-CoV-2: A review of viral, host, and environmental factors, Ann Intern Med 174 (1) (2021) 69–79.
[19] W. Trypsteen, J. Van Cleemput, W.V. Snippenberg, S. Gerlo, L. Vandekerckhove, C.B. Wilen, On the whereabouts of SARS-CoV-2 in the human body: A systematic review, PLoS Pathog 16 (10) (2020) e1009037, https://doi.org/10.1371/journal.ppat.1009037.
[20] E. Cesewski, B.N. Johnson, Electrochemical biosensors for pathogen detection, Biosens Bioelectron 159 (2020) 112214, https://doi.org/10.1016/j.bios.2020.112214.

[21] L.A. Layqah, S. Eissa, An electrochemical immunosensor for the corona virus associated with the Middle East respiratory syndrome using an array of gold nanoparticle-modified carbon electrodes, Mikrochim Acta 186 (4) (2019) 224.
[22] T. Dastagir, E.S. Forzani, R. Zhang, I. Amlani, L.A. Nagahara, R. Tsui, N. Tao, Electrical detection of hepatitis C virus RNA on single wall carbon nanotube-field effect transistors, Analyst 132 (8) (2007) 738–740.
[23] M. Sayhi, O. Ouerghi, K. Belgacem, M. Arbi, Y. Tepeli, A. Ghram, Ü. Anik, L. Österlund, D. Laouini, M.F. Diouani, Electrochemical detection of influenza virus H9N2 based on both immunomagnetic extraction and gold catalysis using an immobilization-free screen printed carbon microelectrode, Biosens Bioelectron 107 (2018) 170–177.
[24] J. Lin, R. Wang, P. Jiao, Y. Li, Y. Li, M. Liao, Y. Yu, M. Wang, An impedance immunosensor based on low-cost microelectrodes and specific monoclonal antibodies for rapid detection of avian influenza virus H5N1 in chicken swabs, Biosens Bioelectron 67 (2015) 546–552.
[25] W. Shao, M.R. Shurin, S.E. Wheeler, X. He, A. Star, Rapid detection of SARS-CoV-2 antigens using high-purity semiconducting single-walled carbon nanotube-based field-effect transistors, ACS Appl. Mater. Interfaces 13 (8) (2021) 10321–10327.
[26] F. Khosravi, S. Loeian, B. Panchapakesan, Ultrasensitive label-free sensing of IL-6 based on PASE functionalized carbon nanotube micro-arrays with RNA-aptamers as molecular recognition elements, Biosensors (Basel) 7 (4) (2017) 17, https://doi.org/10.3390/bios7020017.
[27] B.C. King, T. Burkhead, B. Panchapakesan, Electrical detection of specific versus non-specific binding events in breast cancer cells, Proc SPIE Int Soc Opt Eng 8460 (2012) 84600S.
[28] F. Khosravi, P. Trainor, S.N. Rai, G. Kloecker, E. Wickstrom, B. Panchapakesan, Label-free capture of breast cancer cells spiked in buffy coats using carbon nanotube antibody micro-arrays, Nanotechnology 27 (13) (2016) 13LT02.
[29] H.K. Choi, J. Lee, M.K. Park, J.H. Oh, Development of single-walled carbon nanotube-based biosensor for the detection of Staphylococcus aureus, J. Food Qual. 2017 (2017) 5239487.
[30] P.G. Collins, K. Bradley, M. Ishigami, A. Zettl, Extreme oxygen sensitivity of electronic properties of carbon nanotubes, Science 287 (5459) (2000) 1801–1804.
[31] P. Stokes, S.I. Khondaker, Local-gated single-walled carbon nanotube field effect transistors assembled by AC dielectrophoresis, Nanotechnology 19 (17) (2008) 175202.
[32] M.B. Lerner, B.R. Goldsmith, R. McMillon, J. Dailey, S. Pillai, S.R. Singh, A.T.C. Johnson, A carbon nanotube immunosensor for Salmonella, AIP Adv. 1 (4) (2011) 042127, https://doi.org/10.1063/1.3658573.
[33] G. Gruner, Carbon nanotube transistors for biosensing applications, Anal. Bioanal. Chem. 384 (2) (2005) 322–335.
[34] C. García-Aljaro, L.N. Cella, D.J. Shirale, M. Park, F.J. Muñoz, M.V. Yates, A. Mulchandani, Carbon nanotubes-based chemiresistive biosensors for detection of microorganisms, Biosens. Bioelectron. 26 (4) (2010) 1437–1441.
[35] J.P. Kim, B.Y. Lee, J. Lee, S. Hong, S.J. Sim, Enhancement of sensitivity and specificity by surface modification of carbon nanotubes in diagnosis of prostate cancer based on carbon nanotube field effect transistors, Biosens Bioelectron 24 (11) (2009) 3372–3378.
[36] I. Heller, A.M. Janssens, J. Männik, E.D. Minot, S.G. Lemay, C. Dekker, Identifying the mechanism of biosensing with carbon nanotube transistors, Nano Lett 8 (2) (2008) 591–595.
[37] W. Tai, L. He, X. Zhang, J. Pu, D. Voronin, S. Jiang, Y. Zhou, L. Du, Characterization of the receptor-binding domain (RBD) of 2019 novel coronavirus: implication for development of RBD protein as a viral attachment inhibitor and vaccine, Cell Mol Immunol 17 (6) (2020) 613–620.
[38] E.V. Suprun, V.V. Shumyantseva, A.I. Archakov, Protein Electrochemistry: Application in Medicine. A Review, Electrochimica Acta 140 (2014) 72–82.
[39] G. Seo, G. Lee, M.J. Kim, S.-H. Baek, M. Choi, K.B. Ku, C.-S. Lee, S. Jun, D. Park, H. G. Kim, S.-J. Kim, J.-O. Lee, B.T. Kim, E.C. Park, S.I. Kim, Rapid detection of COVID-19 causative virus (SARS-CoV-2) in human nasopharyngeal swab specimens using field-effect transistor-based biosensor, ACS Nano 14 (4) (2020) 5135–5142.
[40] F. Krebs, C. Scheller, K. Grove-Heike, L. Pohl, H. Wätzig, Isoelectric point determination by imaged CIEF of commercially available SARS-CoV-2 proteins and the hACE2 receptor, Electrophoresis 42 (6) (2021) 687–692.
[41] G. Qiu, Z. Gai, Y. Tao, J. Schmitt, G.A. Kullak-Ublick, J. Wang, Dual-functional plasmonic photothermal biosensors for highly accurate severe acute respiratory syndrome coronavirus 2 detection, ACS Nano 14 (5) (2020) 5268–5277.
[42] R.L. Pinals, F. Ledesma, D. Yang, N. Navarro, S. Jeong, J.E. Pak, L. Kuo, Y.-C. Chuang, Y.-W. Cheng, H.-Y. Sun, M.P. Landry, Rapid SARS-CoV-2 spike protein detection by carbon nanotube-based near-infrared nanosensors, Nano Lett 21 (5) (2021) 2272–2280.
[43] L.F. de Lima, A.L. Ferreira, M.D.T. Torres, W.R. de Araujo, C. de la Fuente-Nunez, Minute-scale detection of SARS-CoV-2 using a low-cost biosensor composed of pencil graphite electrodes, Proc Natl Acad Sci U S A 118 (30) (2021), https://doi.org/10.1073/pnas.2106724118 e2106724118.
[44] P. Fathi-Hafshejani, N. Azam, L.u. Wang, M.A. Kuroda, M.C. Hamilton, S. Hasim, M. Mahjouri-Samani, Two-Dimensional-Material-Based Field-Effect Transistor Biosensor for Detecting COVID-19 Virus (SARS-CoV-2), ACS Nano 15 (7) (2021) 11461–11469.
[45] E. Gasteiger, A. Gattiker, C. Hoogland, I. Ivanyi, R.D. Appel, A. Bairoch, ExPASy: The proteomics server for in-depth protein knowledge and analysis, Nucleic Acids Res 31 (13) (2003) 3784–3788.